Reactive oxygen species (ROS) generation is stimulated by κ opioid receptor activation through phosphorylated c-Jun N-terminal kinase and inhibited by p38 mitogen-activated protein kinase (MAPK) activation

Selena S. Schattauer[‡], Andrea Bedini[§], Floyd Summers[‡], Aiden Reilly-Treat[‡], Mackenzie M. Andrews[‡¶], Benjamin B. Land[‡], and ⓘ Charles Chavkin[‡1]

From the [‡]Department of Pharmacology, University of Washington School of Medicine, Seattle, Washington 98195, [§]Department of Pharmacy and Biotechnology (FaBiT), University of Bologna, Irnerio, 48-40126 Bologna, Italy, and [¶]Department of Bioengineering, University of Washington College of Engineering, Seattle, Washington 98195

Edited by Roger J. Colbran

Activation of the mitogen-activated protein kinase (MAPK) c-Jun N-terminal kinase (JNK) by the $G_{i/o}$ protein–coupled κ opioid receptor (KOR), μ opioid, and D2 dopamine receptors stimulates peroxiredoxin 6 (PRDX6)-mediated production of reactive oxygen species (ROS). ROS production by KOR-inactivating antagonists norbinaltorphimine (norBNI) and JDTic blocks $G\alpha_i$ protein activation, but the signaling mechanisms and consequences of JNK activation by KOR agonists remain uncharacterized. Binding of arrestins to KOR causes desensitization of G protein signaling and acts as a scaffold to initiate MAPK activation. Here, we found that the KOR agonists U50,488 and dynorphin B stimulated biphasic JNK activation with an early arrestin-independent phase, requiring the small G protein RAC family small GTPase 1 (RAC1) and protein kinase C (PKC), and a later arrestin-scaffolded phase, requiring RAC1 and Ras homolog family member (RHO) kinase. JNK activation by U50,488 and dynorphin B also stimulated PRDX6-dependent ROS production but with an inverted U-shaped dose-response relationship. KOR agonist-induced ROS generation resulted from the early arrestin-independent phase of JNK activation, and this ROS response was suppressed by arrestin-dependent activation of the MAPK p38. The apparent balance between p38 MAPK and JNK/ROS signaling has important physiological implications for understanding of dynorphin activities during the stress response. To visualize these activities, we monitored KOR agonist–mediated activation of ROS in transfected live cells by two fluorescent sensors, CellROX Green and HyPerRed. These findings establish an important aspect of opioid receptor signaling and suggest that ROS induction may be part of the physiological response to KOR activation.

Both κ opioid receptor (KOR)[2] agonists and antagonists have potential therapeutic utilities (1–4). Functionally selective KOR agonists that activate Gβγ signaling without activating p38 MAPK signaling produce analgesia without the dysphoric and anxiogenic effects of unbiased KOR agonists or the proaddictive effects of μ opioid receptor (MOR) agonists (2, 4–10). KOR antagonists can promote stress resilience by blocking endogenous dynorphin peptide actions, which contribute to the dysphoric, anxiogenic, and proaddictive effects of stress exposure (6, 11–16). In support of these preclinical findings, both KOR antagonists and agonists have been advanced in human clinical trials (17, 18). However, the functionally selective signaling responses evoked by KOR activation are incompletely understood, and the rational design of optimal κ therapeutics requires a better understanding of the underlying molecular mechanisms involved.

Many of these signaling mechanisms at the κ receptor have been partially characterized (Fig. 1A): conventional KOR agonist binding results in $G\alpha_{i/o}$·Gβγ activation by stimulating guanine nucleotide (GDP–GTP) exchange typical of G protein–coupled receptors (GPCRs). Sustained KOR activation by high-efficacy agonists induces Gβγ-dependent G protein receptor kinase 3 (GRK3) phosphorylation of KOR and subsequent arrestin association (19, 20). Arrestin binding to KOR sterically blocks G protein association and thereby causes KOR desensitization of that signaling pathway. KOR activation also stimulates other protein kinase cascades, including the mitogen-activated protein kinases (MAPKs). KOR activation of the MAPK ERK1/2 occurs in two phases: an arrestin-independent early phase and an arrestin-dependent late phase (21, 22). In contrast, KOR activation of p38 MAPK occurs solely by the late-phase, arrestin-dependent mechanism (22, 23). Arrestin associated with KOR acts as a kinase scaffold that increases both phospho-ERK (pERK) and phospho-p38 MAPK (pp38). KOR-dependent aversion results from pp38-induced activation of serotonin transport and direct effects of pp38 on ventral tegmental area dop-

---

[2] The abbreviations used are: KOR, κ opioid receptor; MAPK, mitogen-activated protein kinase; MOR, KOR, μ opioid receptor; ROS, reactive oxygen species; JNK, c-Jun N-terminal kinase; ANOVA, analysis of variance; PRDX6, peroxiredoxin 6; RAC1, G protein RAC family small GTPase 1; PKC, protein kinase C; RHO, Ras homolog family member; norBNI, norbinaltorphimine; GPCR, G protein-coupled receptor; GRK, G protein receptor kinase; ERK, extracellular signal-regulated kinase; pERK, phospho-ERK; pp38, phospho-p38 MAPK; IR, immunoreactivity; PTX, pertussis toxin; NAC, N-acetylcysteine; PLA₂, phospholipase A₂; Bis-Tris, 2-[bis(2-hydroxyethyl)amino]-2-(hydroxymethyl)propane-1,3-diol; DAPI, 4′,6-diamidino-2-phenylindole.

amine neuron physiology (8, 24, 25). Additionally, analgesia induced by KOR agonists in females is inhibited by estradiol, which stimulates GRK2 to sequester $G\beta\gamma$ and block arrestin-independent signaling while leaving arrestin-dependent signaling and aversive behaviors largely intact (26).

Recent studies have also demonstrated that receptor binding of either KOR agonists or antagonists activates a third MAPK, c-Jun N-terminal kinase (JNK) by stimulating phosphorylation at Thr-183 and Tyr-185 of JNK-1 (27–29). The selective KOR antagonists norbinaltorphimine (norBNI) and JDTic produce their long-lasting inhibition of KOR signaling following JNK-1 isozyme activation (30), and the molecular mechanisms involved have recently been identified (29). Activation of phospho-JNK by norBNI stimulates peroxiredoxin 6 (PRDX6), which in turn stimulates NADPH oxidase to generate reactive oxygen species (ROS). Local production of ROS oxidizes the cysteine sulfhydryl of $G\alpha_i$ required for reversible palmitoylation. The depalmitoylated $G\alpha_i$ binds tightly to KOR but in a conformation that prevents nucleotide exchange by the KOR signaling complex (29). The tightly bound, depalmitoylated KOR–$G\alpha_i$ complex is permanently inactivated, and recovery presumably requires new receptor synthesis to restore KOR function. Thus, these receptor-inactivating KOR antagonists are actually functional (JNK-biased) agonists that have long durations of effect through a JNK-dependent mechanism rather than through slow drug dissociation (27–31). This form of receptor regulation is likely to be a general property of $G\alpha_{i/o}$ signaling as a similar mechanism was found to mediate morphine tolerance at the μ opioid receptor and quinpirole tolerance at the D2 dopamine receptor (29).

KOR agonists have also been shown to increase phospho-JNK (27, 32, 33), but how this process differs from KOR antagonist mechanisms is unclear, and whether KOR agonist activation of pJNK signaling has other physiological consequences is not known. To address these questions, we have focused on how KOR activation by conventional agonists stimulates JNK signaling. KOR agonists were found to increase phospho-JNK by both arrestin-independent and arrestin-dependent mechanisms. JNK activation by KOR agonists stimulated the production of ROS that could be detected by the fluorescent sensors CellROX Green and HyPerRed in transfected HEK293 cells.

Results

Activation of JNK by the KOR agonist U50,488

HEK293 cells stably transfected with KOR respond to the selective agonist U50,488 (10 μM) with a biphasic increase in phospho-JNK (Fig. 1, *B* and *C*). Phospho-JNK immunoreactivity (IR) was significantly increased in an early phase at 15 min (170 $\pm$ 21% of basal, $p < 0.05$) and significantly increased in a late phase with a peak at 60 min (160 $\pm$ 21% of basal, $p < 0.05$). To confirm that the increase in JNK phosphorylation was mediated through KOR activation of $G\alpha_i$, cells were pretreated with pertussis toxin (PTX; 10 ng/ml) 3 h prior to treatment with 10 μM U50,488 for 15 or 60 min, and cell lysates were immunoblotted for phospho-JNK IR (Fig. 1, *D* and *E*). PTX significantly inhibited U50,488-induced phospho-JNK IR compared with vehicle pretreatment

at both 15 min (104 $\pm$ 4 and 138 $\pm$ 12%, respectively; $p < 0.05$) and 60 min (81 $\pm$ 12 and 126 $\pm$ 7%, respectively; $p < 0.01$). To further confirm agonist-induced JNK activity, we looked at U50,488-mediated phosphorylation of the JNK substrate c-Jun (Fig. 1, *F* and *G*). U50,488 treatment resulted in a monophasic increase in phospho-c-Jun IR with a significant increase at 60 min (172 $\pm$ 18% of basal, $p < 0.01$).

We next sought to replicate these findings with dynorphin B, an endogenous peptide ligand for KOR (34, 35). KOR-expressing HEK293 cells were treated for 5–60 min with 1 μM dynorphin B, and cell lysates were then immunoblotted for phospho-JNK (Fig. 1, *H* and *I*). Similar to U50,488, dynorphin B stimulated a biphasic increase in phospho-JNK IR with significantly increased phospho-JNK IR at 30 min (136 $\pm$ 6% of basal, $p < 0.01$) and 120 min (133 $\pm$ 12% of basal, $p < 0.05$), indicating that JNK activation by dynorphin is qualitatively similar to U50,488 but with slightly delayed kinetics. The reason for the slower kinetics of JNK phosphorylation following dynorphin is unclear as no difference in kinetics is observed in dynorphin-induced ERK1/2 activation (Fig. 1, *J* and *K*).

Mechanisms of JNK activation by KOR

To assess the role of arrestin, we transfected KOR-expressing HEK293 cells with siRNA against arrestin 2, arrestin 3, or scrambled control siRNA prior to treatment with 10 μM U50,488 for 15 or 60 min. Selective knockdown of arrestin 2 or arrestin 3 was confirmed by immunoblotting for each isoform (Fig. 2, *A* and *B*). Arrestin 2 IR was selectively reduced by siRNA against arrestin 2 (48 $\pm$ 2% of control, $p < 0.01$) but not by siRNA against arrestin 3 (98 $\pm$ 16% of control). Arrestin 3 IR was significantly reduced by siRNA against arrestin 3 (38 $\pm$ 6% of basal, $p < 0.001$) but not by siRNA against arrestin 2 (89 $\pm$ 10% of basal). Knockdown of arrestin 2 or 3 had no effect on the early phase (15 min) of U50,488-stimulated phospho-JNK IR compared with control siRNA transfection (135 $\pm$ 12, 133 $\pm$ 8, and 139 $\pm$ 8% of basal, respectively) (Fig. 2, *C* and *D*). In contrast, knockdown of arrestin 3, but not arrestin 2, significantly inhibited the late phase (60 min) of U50,488-stimulated phospho-JNK IR at (102 $\pm$ 12% of basal, $p < 0.05$, and 143 $\pm$ 7% of basal, respectively) compared with control siRNA transfection (133 $\pm$ 5% of basal). These data suggest that the early-phase JNK activation by U50,488 is arrestin-independent, whereas later-phase activation at 60 min depends on arrestin 3 expression.

We next sought to characterize the mechanisms underlying KOR-mediated JNK activation. A role for the small G protein RAC, but not RHO, in KOR-stimulated JNK phosphorylation has been described previously (32). Several studies have also indicated that KOR is capable of stimulating PKC activity (36–40), and PKC activity has been implicated in morphine-stimulated JNK activation (41). Based on these studies, we pretreated KOR-expressing HEK293 cells with 10 μM Y27632 (a selective inhibitor of RHO kinase), 100 μM NSC23766 (a selective inhibitor of RAC1), 5 μM Gö6976 (a PKC inhibitor), or vehicle prior to treatment with 10 μM U50,488 for 15 or 60 min and immunoblotting cell lysates for phospho-JNK IR. NSC23766 and Gö6976 significantly inhibited U50,488-stimulated phospho-JNK IR at 15 min (95 $\pm$ 8% of basal, $p < 0.01$, and 90 $\pm$ 12% of basal, $p < 0.01$, respec-
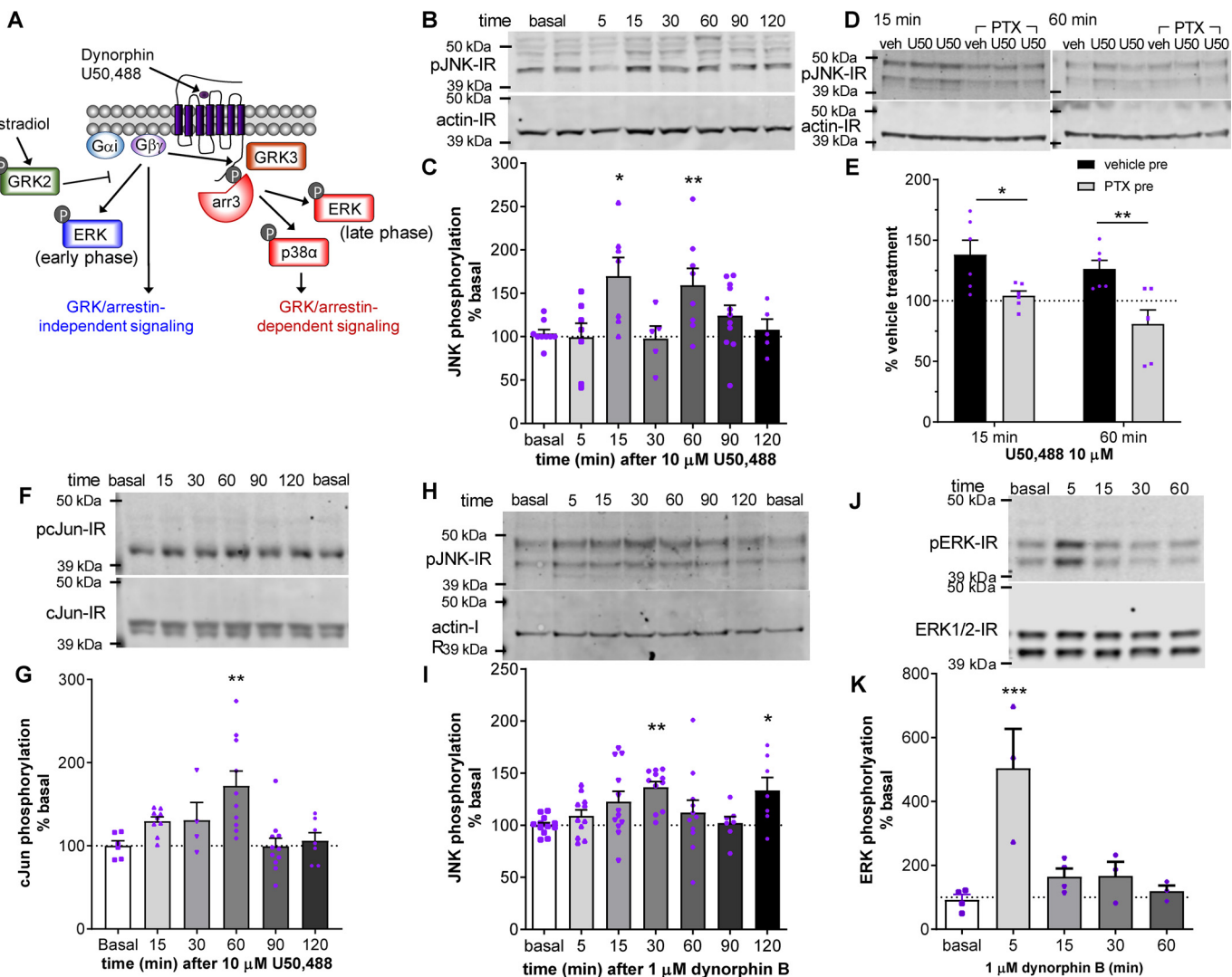
Figure 1. *A–E*, biphasic activation of JNK by U50,488 and dynorphin B. *A*, KOR signals through $G\alpha_{i/o} \cdot G\beta\gamma$ using both arrestin-independent and arrestin-scaffolded pathways as described in the Introduction. *arr*, arrestin. *B* and *C*, HEK293 cells stably expressing KORGFP were treated with 10 μM U50,488 for the indicated time, and cell lysates were immunoblotted for phospho-JNK. Representative immunoblots (*B*) and quantification (*C*) are shown. A significant increase in phospho-JNK immunoreactivity was observed at 15- and 60-min U50,488 treatment (one-way ANOVA ($F_{6,45} = 3.697$, $p = 0.0045$, $n = 5–11$) with Holm–Šidák post hoc comparison against basal (*, $p = 0.0148$ for 15 min and *, $p = 0.0379$ for 60 min)). *D* and *E*, HEK293 cells stably expressing mycKOR were pretreated with 10 ng/ml PTX or vehicle 3 h prior to 15- or 60-min 10 μM U50,488 treatment. Representative immunoblots (*D*) and quantification (*E*) are shown. Pretreatment with PTX significantly inhibited JNK phosphorylation induced by 15- or 60-min U50,488 treatment (two-way ANOVA (significant effect of PTX, $F_{1,20} = 18.51$, $p = 0.0003$, $n = 6$; U50,488 treatment time, $F_{1,20} = 3.622$, $p = 0.0715$; interaction, $F_{1,20} = 0.3873$, $p = 0.5407$) with Holm–Šidák post hoc comparison against vehicle pretreatment (*, $p = 0.017$; **, $p = 0.0047$)). *F–J*, activation of c-Jun by U50,488. *F* and *G*, HEK293 cells stably expressing KORGFP were treated with 10 μM U50,488 for the indicated time, and cell lysates were immunoblotted for phospho-c-Jun. Representative immunoblots (*F*) and quantification (*G*) are shown. A significant increase in phospho-c-Jun immunoreactivity was observed at 60-min U50,488 treatment (one-way ANOVA ($F_{5,42} = 5.142$, $p < 0.0009$, $n = 6–11$) with Holm–Šidák post hoc comparison against basal (**, $p = 0.0038$)). *H* and *I*, HEK293 cells stably expressing mycKOR were treated with 1 μM dynorphin for the indicated time, and cell lysates were immunoblotted for phospho-JNK. Representative immunoblots (*H*) and quantification (*I*) are shown. A significant increase in phospho-JNK immunoreactivity was observed at 30- and 120-min dynorphin B treatment (one-way ANOVA ($F_{6,64} = 2.932$, $p = 0.0137$, $n = 7–12$) with Holm–Šidák post hoc comparison against basal (**, $p = 0.0097$; *, $p = 0.0496$)). *J* and *K*, HEK293 cells stably expressing mycKOR were treated with 1 μM dynorphin B for the indicated time, and cell lysates were immunoblotted for phospho-ERK1/2. Representative immunoblots (*J*) and quantification (*K*) are shown. A significant increase in phospho-ERK1/2 immunoreactivity was observed at 5-min dynorphin treatment (one-way ANOVA ($F_{4,12} = 9.04$, $p = 0.0013$, $n = 3–4$) with Holm–Šidák post hoc against basal (***, $p = 0.0006$)). Graphs depict mean ± S.E. with individual determinations shown.

tively) as compared with vehicle pretreatment (136 ± 4% of basal), but Y27632 had no effect on phospho-JNK IR at this time point (144 ± 16% of basal) (Fig. 2, *E–G*). However, both NSC23766 and Y27632 pretreatment significantly inhibited U50,488-stimulated phospho-JNK IR at 60 min (100 ± 9% of basal, $p < 0.05$, and 98 ± 6%, $p < 0.05$, respectively) as compared with vehicle pretreatment (130 ± 7% of basal) (Fig. 2, *H* and *J*). In contrast, the PKC inhibitor Gö6976 did

not block, and in fact potentiated, U50,488-stimulated phospho-JNK IR at 60 min (175 ± 17% of basal, $p < 0.01$) (Fig. 2, *I* and *J*). These data implicate the RAC family of small G proteins in the arrestin-independent activation of JNK by U50,488 at 15 min but both the RHO and RAC families of small G protein in arrestin-dependent phase activation of JNK at 60 min. These results also provide evidence that PKC is required for arrestin-independent JNK activation but not
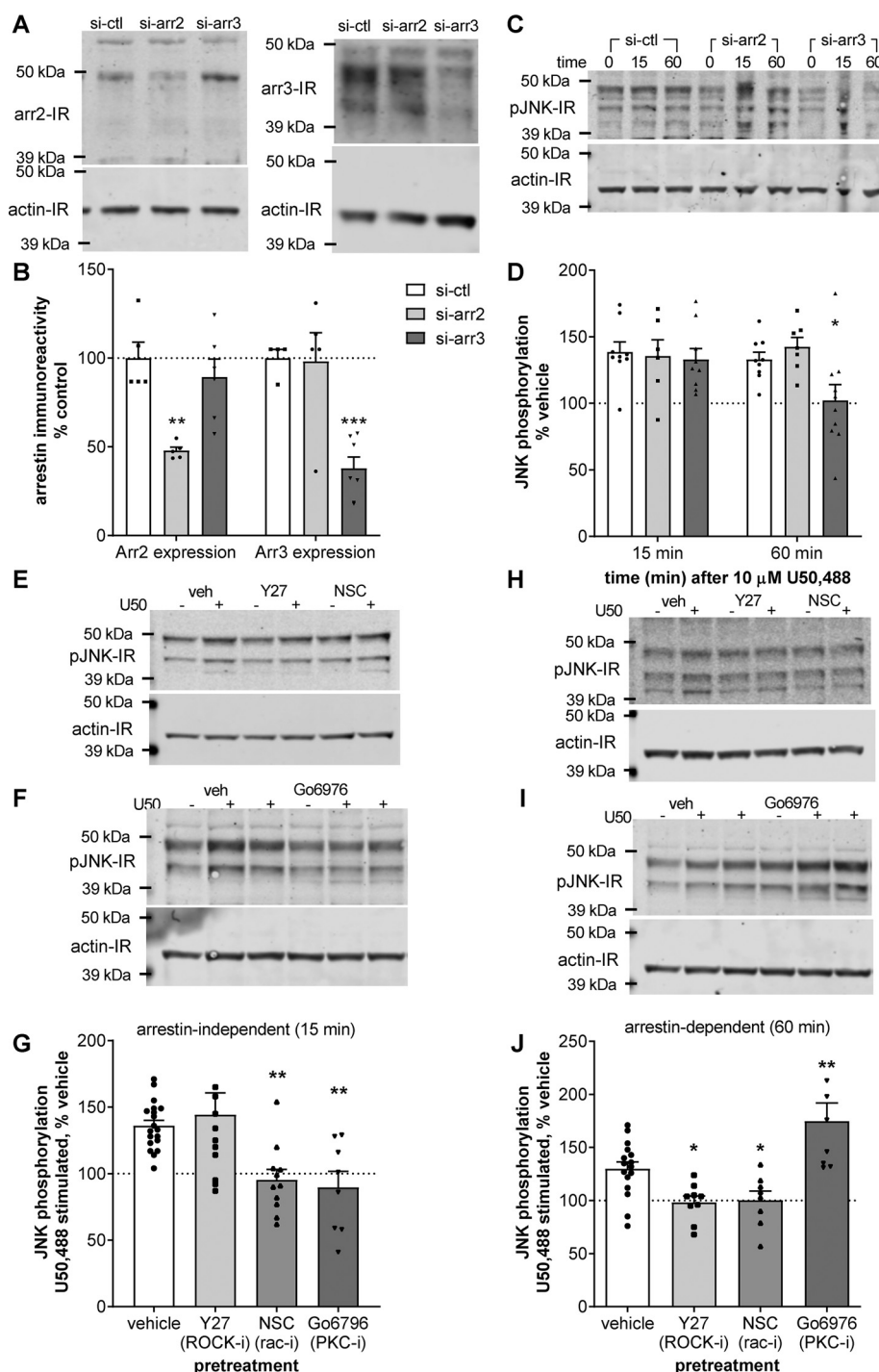
Figure 2. Arrestin-independent and -dependent U50,488 stimulated phospho-JNK occur by distinct mechanisms. *A–D*, HEK293 cells stably expressing KORGFP were treated transfected with control siRNA (*si-ctl*), siRNA against arrestin 2 (*si-arr2*), or siRNA against arrestin 3 (*si-arr3*) 48 h prior to treatment with vehicle or 10 μM U50,488 for 15 or 60 min. Cell lysates were then immunoblotted. *A* and *B*, knockdown of arrestin (*arr*) 2 and 3 was confirmed by immunoblotting. Representative immunoblots (*A*) and quantification (*B*) are shown (two-way ANOVA (significant effect of siRNA, $F_{2,26} = 2.711$, $p = 0.0023$, and significant interaction between siRNA and arrestin isoform, $F_{2,26}$, $p < 0.0001$; $n = 4–7$; arrestin expression, $F_{1,26} = 0.003077$, $p = 0.9562$) with Holm–Šidák post hoc comparison against control siRNA (**, $p = 0.0015$; ***, $p = 0.0002$)). *C* and *D*, cell lysates were immunoblotted for phospho-JNK. Representative immunoblots (*C*) and quantification (*D*) are shown. Transfection with siRNA against arrestin 3 significantly blocked JNK phosphorylation after 15-min U50,488 treatment (two-way ANOVA (significant effect of arrestin, $F_{2,44} = 3.312$, $p = 0.0457$, $n = 6–10$; effect of treatment time, $F_{1,44} = 1.703$, $p = 0.1987$; effect of interaction, $F_{2,44} = 2.227$, $p = 0.1199$) with Holm–Šidák post hoc comparison against control siRNA (*, $p = 0.0277$)). *E–G*, HEK293 cells stably expressing KORGFP were pretreated with 10 μM Y27632 (*Y27*), 100 μM NSC23766 (*NSC*), 5 μM Gö6976, or vehicle (*veh*) minutes prior to 15-min 10 μM U50,488 (*U50*) treatment. Representative immunoblots (*E* and *F*) and quantification (*G*) are shown. Pretreatment with NSC23766 or Gö6976, but not Y27632, significantly blocked stimulation of phospho-JNK by U50,488 at 15 min (one-way ANOVA ($F_{3,46} = 7.026$, $p = 0.0005$, $n = 8–19$) with Holm–Šidák post hoc comparison against vehicle pretreatment (**, $p = 0.0089$)). *H–J*, cells were treated as for *E–G* but treated with U50,488 for 60 min. Representative immunoblots (*H* and *I*) and quantification (*J*) are shown. Treatment with Y27632 or NSC23766 significantly blocked stimulation of phospho-JNK by U50,488 at 60 min, whereas pretreatment with Gö6976 increased stimulation of phospho-JNK by U50,488 at 60 min (one-way ANOVA ($F_{3,37} = 11.58$, $p < 0.0001$, $n = 8–16$) with Holm–Šidák post hoc comparison against vehicle pretreatment (*, $p = 0.0319$; **, $p = 0.0043$)). Graphs depict mean ± S.E. with individual replicates shown.
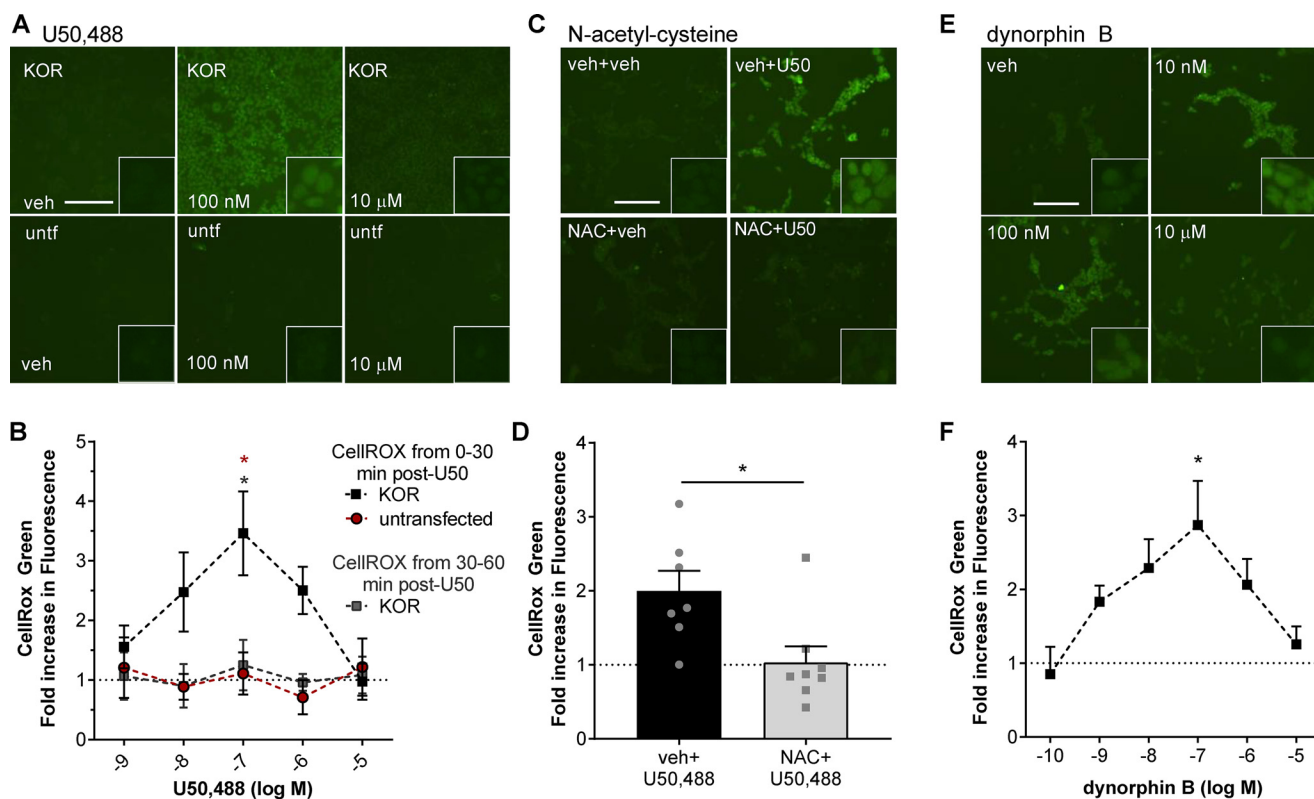
Figure 3. U50,488 and dynorphin B stimulate generation of reactive oxygen species. *A* and *B*, untransfected (*untf*) HEK293 cells or HEK293 cells stably expressing mycKOR were treated with CellROX Green and with the indicated concentration of U50,488 (*U50*) for 30 min or with the indicated concentration of U50,488 for 60 min with CellROX Green added for the last 30 min. Cells were fixed and imaged for CellROX Green fluorescence. Representative images (*A*) and quantification (*B*) are shown. Fluorescence was significantly increased in mycKOR HEK293 cells following 30 min of 100 nM U50,488 treatment (two-way ANOVA (significant effect of group, $F_{2,42} = 9.749$, $p = 0.0003$, $n = 3–6$; effect of concentration, $F_{2,42} = 1.206$, $p = 0.3226$; and interaction effect, $F_{8,42} = 1.471$, $p = 0.1969$) with Holm–Šidák post hoc against untransfected cells and later CellROX treatment (*red* *, $p = 0.0246$ and *gray* and *red* *, $p = 0.0211$). *C* and *D*, cells were pretreated with 10 μM NAC or vehicle (*veh*) for 30 min. Cells were then treated with CellROX Green and 100 nM U50,488 for 30 min. Cells were fixed and imaged for CellROX Green fluorescence. Representative images (*C*) and quantification (*D*) are shown. Pretreatment with NAC significantly blocked U50,488-stimulated CellROX Green fluorescence (Student's *t* test, $p = 0.0151$, $n = 7–8$). *E* and *F*, cells were treated as for *A* but with the indicated concentration of dynorphin B. Fluorescence was significantly increased in mycKOR HEK293 cells following 30-min 100 nM dynorphin B treatment. Representative images (*E*) and quantification (*F*) are shown (one-way ANOVA ($F_{5,42} = 2.514$, $p = 0.0444$, $n = 4–10$) with Holm–Šidák post hoc comparison against 0.1 nM (*, $p = 0.0149$)). *Scale bars* represents 200 μm (50 μm for *inset*); graphs depict mean ± S.E. with individual replicates shown.

arrestin-dependent JNK activation, in agreement with our similar studies on the μ opioid receptor (41).

Generation of reactive oxygen species is induced by KOR agonists

JNK activation by long-acting KOR antagonists results in receptor inactivation through a PRDX6–ROS-mediated depalmitoylation mechanism (29), but it is unclear whether JNK activation by conventional KOR agonists also stimulates ROS production. Using CellROX Green (a cell-permeable dye that fluoresces upon oxidation-induced nucleic acid binding, which is not readily reversible) to detect ROS production, KOR-expressing HEK293 cells or untransfected control HEK293 cells were incubated with CellROX Green and U50,488 (concentration range, 1 nM to 10 μM), fixed, and imaged for CellROX Green fluorescence (Fig. 3, *A* and *B*). U50,488 treatment resulted in a significant increase of CellROX Green fluorescence in the first 30 min in KOR-expressing cells but not in untransfected HEK293 cells ($p < 0.01$). In contrast, no increase in fluorescence was observed in KOR-expressing cells that were incubated with CellROX Green from 30 to 60 min after U50,488 (Fig. 3*B*). Interestingly, U50,488 stimulated ROS generation with an inverted U-shaped dose response with peak

fluorescence at 100 nM (3.5 ± 1.6-fold over vehicle, $p < 0.05$ *versus* untransfected) and no change in fluorescence intensity after treatment with 10 μM U50,488 (1.0 ± 0.6-fold over vehicle). No changes in CellROX Green fluorescence were observed at any concentration of U50,488 in untransfected HEK293 cells, demonstrating that this inverted U-shaped dose-response relationship was not a result of off-target effects. To confirm that the changes in CellROX Green fluorescence were due to increases in ROS, KOR-expressing HEK293 cells were pretreated with 10 μM *N*-acetylcysteine (NAC; a nonselective antioxidant) or vehicle prior to treating cells for 30 min with 100 nM U50,488 in the presence of CellROX Green (Fig. 3, *C* and *D*). U50,488-stimulated CellROX Green fluorescence was significantly inhibited by NAC pretreatment (1.0 ± 0.2-fold of vehicle-treated, $p < 0.05$) as compared with vehicle pretreatment (2.0 ± 0.3-fold of vehicle treatment).

Based on these results, we predicted that treatment with the endogenous KOR ligand dynorphin B would also induce ROS generation. KOR-expressing HEK293 cells were treated with dynorphin B (concentration range, 100 pM to 10 μM) for 30 min in the presence of CellROX Green; cells were then fixed and imaged for CellROX Green fluorescence (Fig. 3, *E* and *F*). As
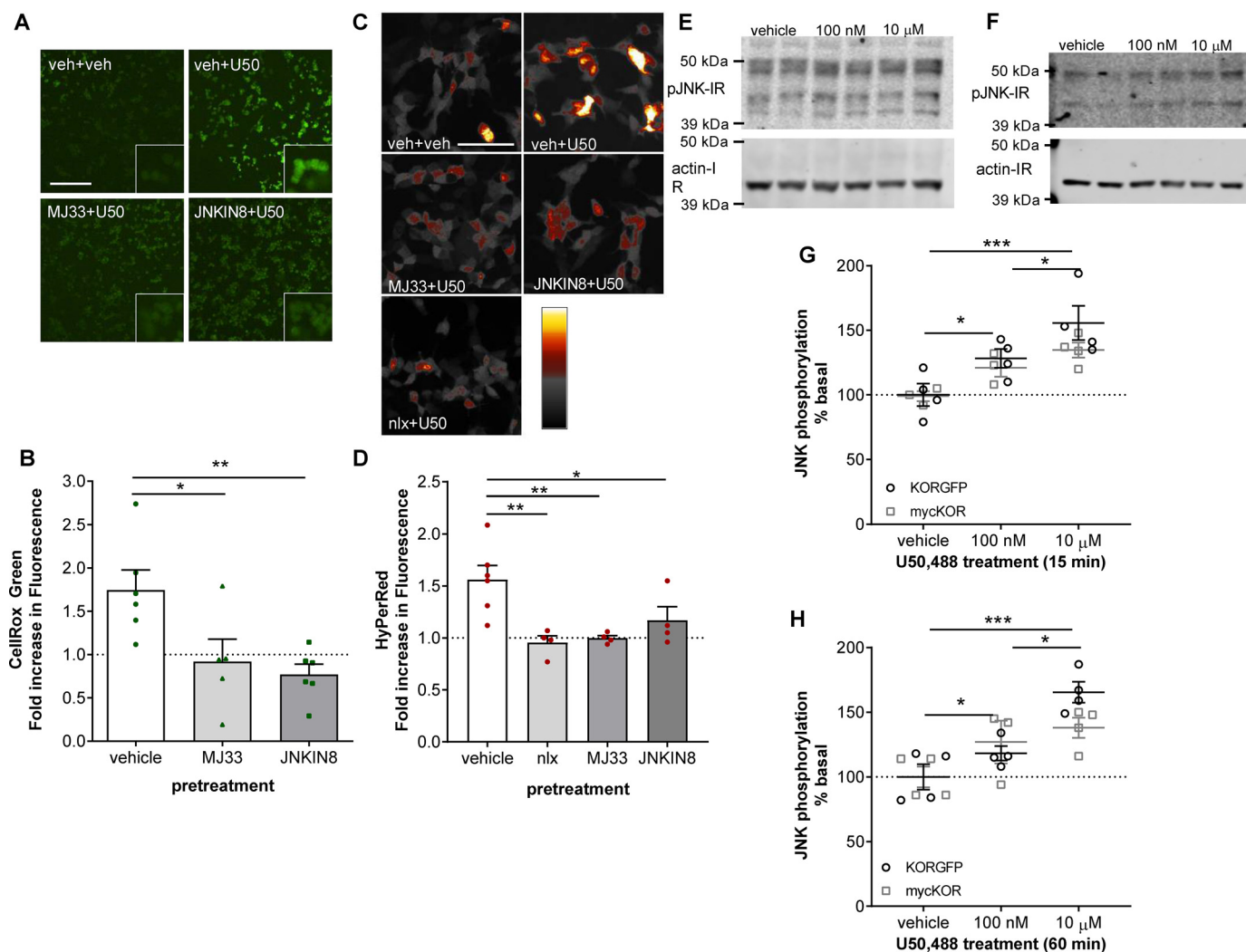
Figure 4. U50,488 stimulated reactive oxygen species generation is PRDX6 and JNK mediated. *A* and *B*, HEK293 cells stable expressing mycKOR were pretreated with 10 μM MJ33, 1 μM JNK-IN-8, or vehicle (*veh*) for 15 min. Cells were then treated with CellROX Green and 100 nM U50,488 (*U50*) for 30 min. Cells were fixed and imaged for CellROX Green fluorescence. Representative images (*A*) and quantification (*B*) are shown. The *scale bar* represents 200 μm (50 μm for *inset*). MJ33 or JNK-IN-8 pretreatment significantly blocked U50,488-stimulated CellROX Green fluorescence (one-way ANOVA ($F_{2,14} = 6.682$, $p = 0.0084$, $n =$ 5–6) with Holm–Šidák post hoc against vehicle pretreatment (*, $p = 0.0142$; **, $p = 0.0075$)). *C* and *D*, HEK293 cells stably expressing mycKOR were transiently transfected with HyPerRed 24–36 h prior to the experiment. Cells were pretreated with 10 μM MJ33, 1 μM JNK-IN-8, 10 μM naloxone, or vehicle for 15 min prior to treatment with 100 nM U50,488 for 30 min. Cells were fixed and imaged for HyPerRed fluorescence. Representative images (*C*) and quantification (*D*) are shown. The *scale bar* represents 100 μM. MJ33, JNK-IN-8, or naloxone (*nlx*) pretreatment significantly blocked U50,488-stimulated HyPerRed fluorescence (one-way ANOVA ($F_{3,14} = 6.786$, $p = 0.0047$, $n = 4$–6) with Holm–Šidák post hoc against vehicle pretreatment (*, $p = 0.0249$; **, $p = 0.0056$ for MJ33 and **, $p =$ 0.0049 for naloxone)). *E*–*H*, HEK293 cells stably expressing mycKOR or KORGFP were treated with vehicle or 100 nM or 10 μM U50,488 for 15 (*E* and *G*) or 60 (*F* and *H*) min, and cell lysates were immunoblotted for phospho-JNK. Representative immunoblots (*E* and *F*) are shown. *G*, quantification of phospho-JNK IR after 15-min treatment (two-way ANOVA (significant effect of treatment, $F_{2,16} = 13.93$, $p = 0.0003$, but not receptor, $F_{1,16} = 1.85$, $p = 0.1927$, or interaction, $F_{2,16} =$ 0.7084, $p = 0.5072$, $n = 3$–4) with Holm–Šidák post hoc comparison between each concentration (*, $p = 0.0259$ for 100 nM and *, $p = 0.0302$ for 10 μM; ***, $p =$ 0.0002)). *H*, quantification of phospho-JNK IR after 60-min treatment (two-way ANOVA (significant effect of treatment, $F_{2,17} = 16.76$, $p < 0.0001$, but not receptor, $F_{1,17} = 0.6916$, $p = 0.4171$, or interaction, $F_{2,17} = 2.124$, $p = 0.1502$, $n = 3$–4) with Holm–Šidák post hoc comparison between each concentration (*, $p = 0.0267$ for 100 nM and *, $p = 0.0123$ for 10 μM; ***, $p < 0.0001$)). Graphs depict mean ± S.E. with individual replicates shown.

observed with U50,488, dynorphin B stimulated ROS generation with an inverted U-shaped dose response. Peak fluorescence was observed at 100 nM (2.9 ± 0.6-fold over vehicle, $p < 0.05$ *versus* 0.1 nM), and there was no change in fluorescence after treatment with 10 μM dynorphin B (1.3 ± 0.2-fold over vehicle).

Mechanism of reactive oxygen species stimulation by KOR

To determine whether JNK and the phospholipase A_2 (PLA_2) activity of PRDX6 are also required for U50,488-stimulated ROS production, we pretreated KOR-expressing HEK293 cells with 10 μM MJ33 (an inhibitor of PRDX6 PLA_2 activity) (42–44), 1 μM JNK-IN-8 (a JNK inhibitor) (45), or

vehicle prior to treating cells for 30 min with 100 nM U50,488 in the presence of CellROX Green. Cells were then fixed and imaged for CellROX Green fluorescence (Fig. 4, *A* and *B*). U50,488-stimulated CellROX Green fluorescence was significantly inhibited by either MJ33 (0.9 ± 0.3-fold of vehicle-treated, $p < 0.05$) or JNK-IN-8 (0.8 ± 0.1-fold of vehicle-treated, $p < 0.01$) as compared with vehicle pretreatment (1.7 ± 0.2-fold of vehicle treatment).

To extend these results, we transfected KOR-expressing cells with the genetically encoded reversible ROS sensor HyPerRed (46) and tested the effect of pretreatment with 1 μM JNK-IN-8,

10 μM MJ33, or 10 μM naloxone (a nonselective opioid antagonist that does not activate JNK (27–29)) on HyPerRed fluorescence 30 min after treatment with 100 nM U50,488 (Fig. 4, *C and D*). As with the CellROX Green assay, U50,488-induced HyPerRed fluorescence was significantly inhibited by either JNK-IN-8 (1.2 ± 0.1-fold of vehicle-treated, $p < 0.05$) or MJ33 (1.0 ± 0.03-fold of vehicle-treated, $p < 0.01$) as compared with vehicle pretreatment (1.6 ± 0.1-fold of vehicle treatment). These results demonstrate that U50,488 stimulated generation of ROS via JNK and PRDX6, similar to norBNI and morphine (29). Naloxone also blocked HyPerRed fluorescence induced by U50,488 (1.0 ± 0.1-fold of vehicle-treated, $p < 0.01$), further confirming that ROS generation was KOR-mediated.

Because U50,488-stimulated ROS was JNK-dependent, we tested whether JNK phosphorylation induced by U50,488 also followed an inverted U-shaped response by treating KOR-expressing HEK293 cells with two different concentrations of U50,488 for 15 min (Fig. 4, *E and G*). Both 100 nM and 10 μM U50,488 resulted in significant increases in phospho-JNK IR at 15 min (125 ± 5% of vehicle, $p < 0.05$, and 145 ± 8% of vehicle, $p < 0.001$, respectively) with significantly greater IR at 10 μM as compared with 100 nM U50,488 treatment ($p < 0.05$). Furthermore, a similar concentration-dependent increase in phospho-JNK IR following 60-min treatment with 100 nM and 10 μM U50,488 (123 ± 4% of vehicle, $p < 0.05$, and 158 ± 14% of vehicle, $p < 0.001$, respectively) with significantly greater IR at 10 μM as compared with 100 nM U50,488 treatment ($p < 0.05$) (Fig. 4, *F and H*) was also observed. These results suggest that the U-shaped dose response of ROS activation by KOR was not due to decreased JNK activation at higher agonist concentrations.

Reactive oxygen species stimulation by KOR is antagonized by the GRK pathway

Based on the time course of ROS generation, we hypothesized that ROS generation was mediated through the earlier, arrestin-independent phase of JNK activation. To test this, HEK293 cells were transiently transfected with KOR or KOR(S369A), a receptor mutant form that cannot be phosphorylated by GRK3 or recruit arrestin (47, 48), and then treated with U50,488 (1 nM–10 μM) for 30 min in the presence of CellROX Green (Fig. 5, *A and B*). As observed in stable KOR-expressing cells, transiently transfected KOR HEK293 cells responded to U50,488 with an increase in CellROX Green fluorescence. The U50,488 dose response also had an inverted U-shaped dose response peaking at 100 nM (1.9 ± 0.4-fold of vehicle-treated). In contrast, U50,488 did not produce a U-shaped dose response in HEK293 cells transiently transfected with KOR(S369A) cells but instead showed a linear increase in response with increasing dose (Fig. 5B). Higher concentrations (10 μM) of U50,488 produced greater CellROX Green fluorescence (2.8 ± 0.8-fold over vehicle, $p < 0.01$) compared with KOR-expressing cells. These results support the hypothesis that ROS generation was mediated by the arrestin-independent phase of JNK activation as KOR(S369A) solely activates arrestin-independent signaling.

It was not clear why arrestin-dependent JNK activation was unable to activate ROS as the late phase–generated phospho-

JNK should be able to readily diffuse away from the receptor complex and interact with PRDX6 or why high concentrations of drug resulted in a complete loss of ROS activation, which we have not observed for other KOR signaling pathways (10, 22, 23, 27). Furthermore, classic arrestin-mediated GPCR desensitization mechanisms did not clearly explain the loss of ROS stimulation as upstream JNK activation was maintained. An alternative hypothesis is that, following recruitment to KOR, arrestin also acts as a scaffold for activation of p38α MAPK (23, 49), and phospho-p38 has been shown to inhibit JNK in other systems (50). To test the role of phospho-p38 in the ROS response to U50,488, KOR-expressing cells were pretreated with the p38 inhibitor SB203580 (10 μM) or vehicle prior to treating cells for 30 min with 100 nM or 10 μM U50,488 (Fig. 5, *C and D*). SB203580 had no effect on the CellROX Green response to 100 nM U50,488 (2.1 ± 0.3- and 2.5 ± 0.4-fold over vehicle, respectively). However, a significant increase in 10 μM U50,488–stimulated CellROX Green fluorescence was observed in cells pretreated with SB203580 instead of vehicle (2.1 ± 0.3- and 0.75 ± 0.1-fold of vehicle, respectively; $p < 0.05$). Consistent with this explanation, KOR(S369A) does not activate p38 MAPK and hence does not produce an inverted U-shaped dose response. These results suggest that GRK-dependent activation of p38, rather than receptor phosphorylation or arrestin recruitment *per se*, inhibits ROS generation at higher concentrations of agonist. In contrast, no effect of SB203580 was observed on CellROX Green fluorescence stimulated by the KOR ligand norBNI, which has functional selectivity for the JNK–ROS pathway and does not activate arrestin-dependent p38 signaling (Fig. 5, *E and F*) (27–30).

Real-time measurement of reactive oxygen species following KOR agonist

The results described above suggested that ROS generation by KOR agonists may have physiological effects and that live-cell imaging could reveal the kinetics of KOR signaling. To assess this possibility, we next used live-cell imaging of HyPer-Red in KOR-expressing HEK293 cells. Live-cell imaging showed that 100 nM U50,488 elevated ROS at 30 min, and ROS remained elevated at 45 min post-drug application (Fig. 6, *A and C*). Live imaging also revealed that U50,488 induced a transient decrease in HyPerRed fluorescence peaking at ~2–3 min, an effect that was not resolved in the initial studies performed in fixed cells. Both the transient decrease and longer-lasting elevation in ROS, as measured by HyPerRed fluorescence, were blocked by pretreatment with 10 μM naloxone (Fig. 6, *B and D*). In addition, treatment with 10 μM naloxone 30 min after U50,488 activation of HyPerRed fluorescence completely reversed the increase within 15 min after the addition of naloxone (Fig. 6D). This result indicates that the increase in HyPerRed fluorescence required continuing KOR-stimulated ROS production.

Discussion

The key finding of this study is that conventional KOR agonists stimulate ROS generation through a JNK–PRDX6 pathway. This study identified biphasic activation of JNK by KOR agonists through two distinct G protein–dependent mechanisms: an early arrestin-independent pathway and a slower
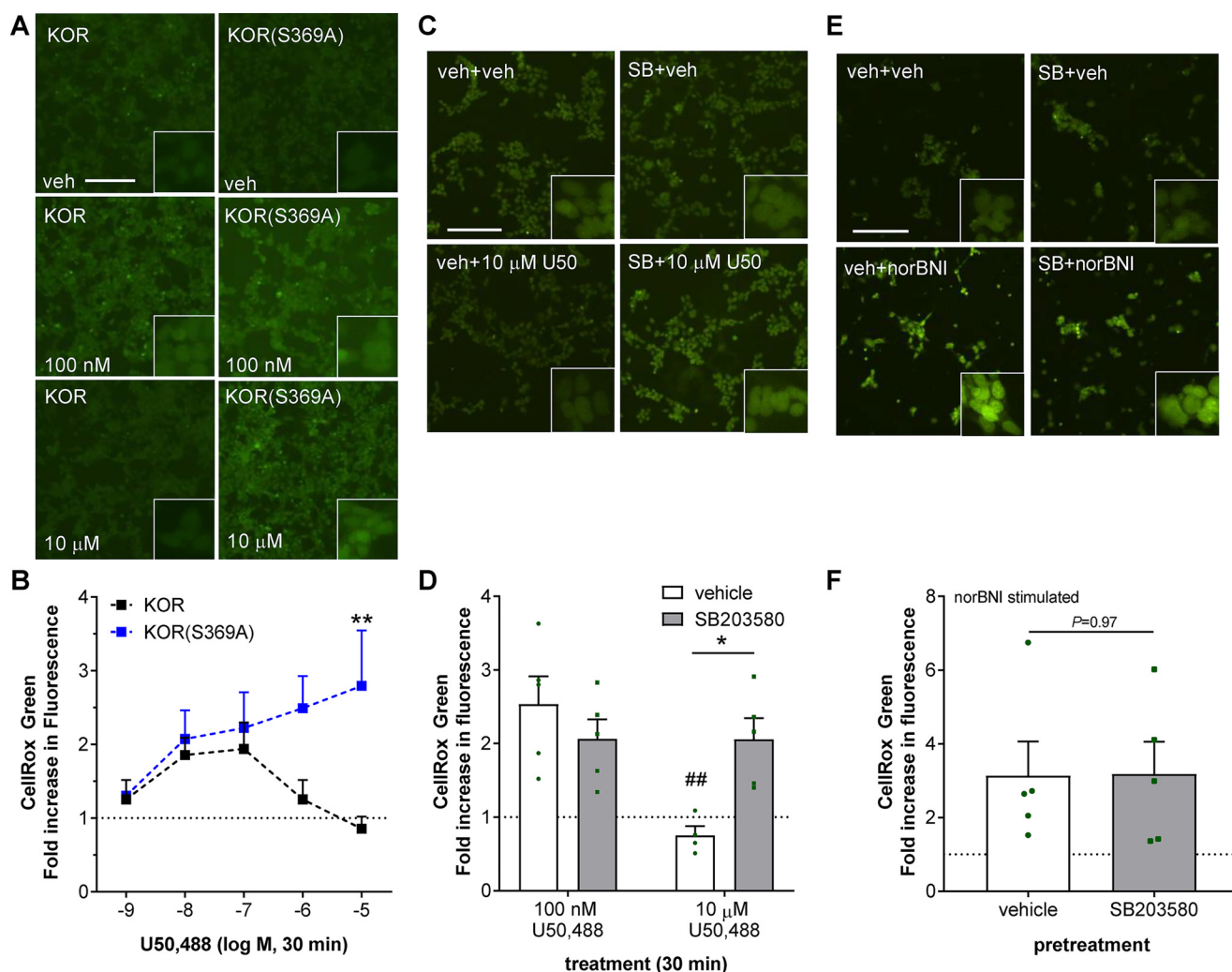
Figure 5. U50,488 stimulated reactive oxygen species generation is inhibited by GRK/arrestin dependent p38 activation. *A* and *B*, untransfected HEK293 cells were transiently transfected with mycKOR or mycKOR(S369A) 24–36 h prior to the experiment. Cells were treated with CellROX Green and the indicated concentration of U50,488 (*U50*) for 30 min, fixed, and imaged for CellROX Green fluorescence. Representative images (*A*) and quantification (*B*) are shown. Fluorescence was significantly greater in mycKOR(S369A)- than mycKOR-transfected HEK293 cells following 30-min 1–10 μM U50,488 treatment (two-way ANOVA (significant effect of receptor, $F_{1,50} = 9.034$, $p = 0.0041$; effect of drug concentration, $F_{4,50} = 1.175$, $p = 0.3331$, and interaction, $F_{4,50} = 2.212$, $p = 0.081$; $n = 6-7$) with Holm–Šidák post hoc against KOR (**, $p < 0.01$)). *C* and *D*, HEK293 cells stable expressing mycKOR were pretreated with 10 μM SB203580 (*SB*) or vehicle (*veh*) for 15 min. Cells were then treated with CellROX Green and 100 nM U50,488 for 30 min. Cells were fixed and imaged for CellROX Green fluorescence. Representative images (*C*) and quantification (*D*) are shown (two-way ANOVA (significant effect of concentration, $F_{1,15} = 9.327$, $p = 0.008$, and significant interaction, $F_{1,15} = 9.203$, $p = 0.0084$; effect of p38 inhibitor, $F_{1,15} = 2.024$, $p = 0.1753$; $n = 4-5$) with Holm–Šidák post hoc against vehicle pretreatment (*, $p < 0.05$) and against 100 nM U50,488 treatment (##, $p < 0.01$)). *E* and *F*, HEK293 cells stably expressing mycKOR were pretreated with 10 μM SB203580 for 15 min. Cells were then treated with 10 μM norBNI for 60 min with CellROX Green for the last 30 min of norBNI treatment. Cells were fixed and imaged for CellROX Green fluorescence. Representative images (*E*) and quantification (*F*) are shown. Pretreatment with SB203580 had no significant effect on CellROX Green fluorescence (Student's *t* test; $n = 6$). *Scale bars* represents 200 μm (50 μm for *inset*); graphs depict mean ± S.E., with individual replicates shown.

arrestin-scaffolded pathway. Induction of ROS generation was mediated by arrestin-independent JNK activation and inhibited by GRK/arrestin-dependent stimulation of p38 activity. JNK-dependent ROS activation is likely to be a general mechanism of $G\alpha_{i/o}$ receptor signaling, representing another aspect of GPCR signaling through $G\alpha_i$, as other members of this receptor family (*e.g.* μ opioid, D2 dopamine, and CB1 cannabinoid receptors) show similar activation of ROS (29).[3]

The initial arrestin-independent JNK phosphorylation required PKC and the small G protein RAC but not RHO. This pathway likely corresponds to the Src and RAC/CDC42-dependent mechanism reported by Kam *et al.* (32). Arrestin-inde-

pendent, PKC-dependent JNK phosphorylation is also stimulated by morphine-like agonists of MOR (41). Previous investigators reported PKC-mediated KOR signaling and desensitization (36–40), and our data link these two pathways. In contrast, arrestin-dependent activation of JNK by U50,488 required both RAC and the RHO effector ROCK1. Unlike the early-phase JNK phosphorylation but similar to arrestin-dependent JNK phosphorylation by the MOR agonist fentanyl (41), PKC was not required. Rather, inhibition of PKC enhanced arrestin-dependent JNK phosphorylation, suggesting that PKC inhibits arrestin-mediated JNK phosphorylation by receptor desensitization or another mechanism.

U50,488 was also found to stimulate increased ROS in a PRDX6 PLA$_2$ activity–dependent manner. These results are

---

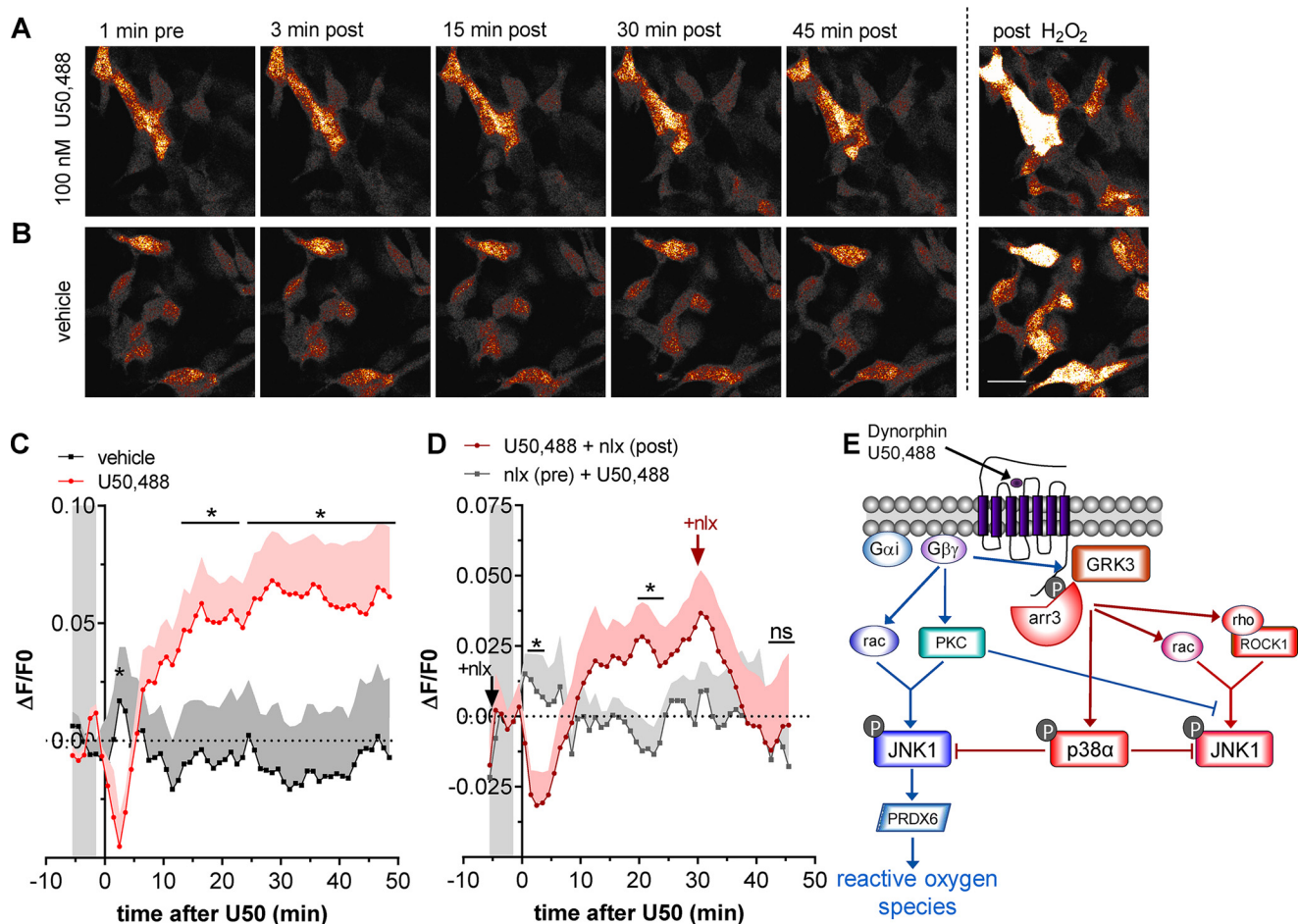[3] S. S. Schattauer, and C. Chavkin, unpublished observations.

Figure 6. U50,488 stimulates ROS in live cells and is reversed by naloxone. *A* and *B*, HEK293 cells stably expressing mycKOR were transiently transfected with HyPerRed 24 h prior to imaging for HyPerRed fluorescence every 60 s. Cells were treated with 100 nм U50,488 (*A*) or vehicle (*B*), and fluorescence was quantified. At the end of the experiment, cells were treated with 200 μм H_2O_2 to confirm responsiveness. The *scale bar* represents 25 μm for images in both *A* and *B*. *C*, quantification of data in *A* and *B*. Fluorescence was significantly increased by U50,488 in mycKOR-expressing HEK293 cells (repeated-measures two-way ANOVA (significant effect of time, $F_{54,432} = 2.531$, $p < 0.0001$ and significant interaction between time and drug, $F_{54,432} = 3.948$, $p < 0.0001$; effect of drug, $F_{1,8} = 2.907$, $p = 0.1324$; $n = 9$) with Holm–Šidák post hoc comparison against vehicle (*, $p < 0.05$)). The graph depicts mean ± S.E. *D*, cells were pretreated with 10 μм naloxone (*nlx*) or vehicle 5 min prior to treatment with 100 nм U50,488; cells were post-treated with vehicle or 10 μм naloxone 30 min after U50,488 (*U50*). 45 min after U50,488 treatment, cells were treated with 200 μм H_2O_2. Fluorescence was significantly increased after U50,488 treatment in mycKOR-expressing HEK293 cells that were not pretreated with naloxone (repeated-measures two-way ANOVA (significant interaction between time and drug, $F_{51,306} = 3.475$, $p < 0.0001$; effect of time, $F_{51,306} = 0.9146$, $p = 0.6409$; effect of drug, $F_{1,6} = 0.8464$, $p = 0.3931$; $n = 7$) with Holm–Šidák post hoc comparison against naloxone pretreatment (*, $p < 0.05$; *ns*, not significant)). *E*, schematic of JNK signaling by KOR agonists. KOR activation promotes analgesia and cognitive disruptions through G protein–mediated mechanisms, including regulation of various ion channels, adenylyl cyclase, and ERK1/2 MAPK. G protein–dependent GRK3 phosphorylation of KOR at Ser-369 promotes arrestin (*arr*) recruitment, resulting in arrestin-scaffolded p38 MAPK activation and aversion in addition to receptor desensitization. This study describes another aspect of signaling in which $\beta\gamma$ subunits also promote JNK activation through G protein–mediated activation of RAC1 and PKC, resulting in increased oxidative signaling via PRDX6 PLA₂ activity. This pathway is directly inhibited by G protein–mediated, arrestin-scaffolded activation of p38 MAPK.

analogous to the previously published findings of JNK/PRDX6-induced ROS by the MOR agonist morphine, which stimulates JNK phosphorylation by an arrestin-independent mechanism (29, 41). Unlike morphine, U50,488 and dynorphin B both stimulated ROS generation with a complex concentration response. Maximal ROS generation was observed at moderate concentrations with a loss of ROS stimulation at receptor-saturating concentrations as a result of receptor phosphorylation by GRK and downstream p38 activity. Inhibition of JNK by p38 explains the lack of ROS generation by the arrestin-dependent JNK pathway observed in this study and previously (29). Based on this, we would predict that partial or G protein–biased agonists might be more efficacious at promoting ROS generation. We would further predict that system biases toward or against GRK–

arrestin pathways would change the extent to which JNK–ROS signaling is activated.

GPCR signaling has been broadly divided into two branches: arrestin-independent signaling, historically referred to as G protein–dependent signaling (51) (including KOR-induced ERK1/2 MAPK phosphorylation and ion-channel modulation), and arrestin-dependent signaling, which requires G proteins as well but is also dependent on arrestin scaffolding of signaling complexes to facilitate signal transduction (52) (including KOR-induced p38 MAPK phosphorylation). Similar to other arrestin-independent G protein–initiated signaling cascades that are desensitized by arrestin recruitment, this JNK–ROS cascade is also inhibited by arrestin-mediated signaling but by a different arrestin-dependent mechanism. The opposing bal-

ance between JNK–ROS signaling and GRK–arrestin–p38 described here may contribute to differential effects of GPCR activation in different cell types and cellular compartments (53–56), dependent on signalosome composition and local cellular environment.

JNK and oxidative pathways both have established roles in cellular stress pathways (57–59). In addition to their role in oxidative stress, ROS can act as signaling molecules, regulating tyrosine phosphorylation, small G protein activity, and transcription factor complexes (60, 61). ROS have also recently been shown to promote desensitization and tolerance for GPCRs, including MOR and KOR (29, 62–64), and adversely affect pain management by opioids. The insights from this study add further clarity to our understanding of functional selectivity at opioid receptors and how the dynorphin–KOR system may contribute to the stress-induced vulnerability to neurodegeneration, mood disorders, and cardiovascular disease (65–68). Markers of oxidative stress are altered in clinical studies and rodent models of psychiatric stress, and ROS have been linked to neurodegenerative disease, pathological pain, and psychiatric disease (67–69); this study suggests that the dynorphin–KOR axis may play an important role in these effects. Further studies will be needed to understand under what conditions ROS is generated by KOR and what roles KOR-induced ROS play in the stress response, aided by the signaling insights and tools validated in this study.

Experimental procedures

Drugs

(−)-U50,488 (Tocris), MJ33 (Sigma-Aldrich), naloxone (NIDA Drug Supply), Y27632 (Tocris), NSC23766 (Tocris), *N*-acetyl-L-cysteine (EMD Millipore), and SB203580 HCL (EMD Millipore) were dissolved in H_2O. JNK-IN-8 (Fisher Scientific) and Gö6976 (EMD Millipore) were dissolved in DMSO. Dynorphin B (Tocris) was dissolved in ethanol. Pertussis toxin (EMD Millipore) was diluted from stock 200 μg/ml concentration to 10 μg/ml in H_2O.

Constructs

KORGFP and mycKOR plasmids were generated as described previously (29, 48). To generate mycKOR(Ser369A), KOR(Ser369A) was cloned for KOR(S369A)GFP (48) as described for synthesis of mycKOR (29). The pC1-HyPer-Red plasmid (46) was purchased from Addgene (Addgene number 48249).

Cell culture and transfection

HEK293 cells (American Type Culture Collections) stably expressing KORGFP and mycKOR were generated as described previously (29). HEK293 cells were maintained in Dulbecco's modified medium/F-12 (Fisher Scientific) with 10% fetal bovine serum (Sigma-Aldrich) and penicillin–streptomycin–L-glutamine (Fisher Scientific). HEK293 cells expressing mycKOR or KORGFP were grown in media supplemented with G418 (200 μg/ml) (Fisher Scientific). HEK293 cells transiently expressing mycKOR, mycKOR(S369A), or HyPerRed were generated by transfecting HEK293 cells using FuGENE HD (Promega) according to the manufacturer's instructions.

We confirmed that the two different methods of receptor tagging used in this study (N-terminal myc and C-terminal GFP) did not impact JNK activation by treating mycKOR- and KORGFP-expressing HEK293 with 100 nM and 10 μM U50,488 for 15 or 60 min and immunoblotting for phospho-JNK. Significantly more phospho-JNK IR was observed following 15-min 10 μM U50,488 than 100 nM U50,488 (145 ± 8 and 125 ± 5%, respectively) (Fig. 4, *E* and *G*). Similarly, more phospho-JNK IR was observed following 60-min 10 μM U50,488 than 100 nM U50,488 (152 ± 7 and 122 ± 7%, respectively) (Fig. 4, *F* and *H*). At neither time point was any effect of receptor tagging observed. Based on this, we used mycKOR for all experiments after studies using CellROX Green were initiated.

siRNA

HEK293 cells stably expressing KORGFP were transiently transfected with siRNA against arrestin 2 or arrestin 3 or a scrambled siRNA control (Dharmacon Research, Pittsburgh, PA; 50 nM final concentration; 48 h) using Lipofectamine RNAiMAX (Life Technologies) according to the manufacturer's recommendations and then blotted for arrestin 2 IR or arrestin 3 IR (antibody provided by Dr. Jeffrey Benovic, Thomas Jefferson University, Philadelphia, PA) (1:3000) and actin (Abcam, Cambridge, MA; 1:5000) in 5% BSA-TBST (20 mM Tris, 150 mM NaCl, 0.1% Tween 20, pH 7.2) overnight at 4 °C. Relative fluorescent band intensity was measured using Odyssey software and expressed as arrestin 2 IR or arrestin 3 IR intensity over actin IR intensity and then expressed as normalized to scrambled siRNA treatment.

Western blot analysis

HEK293 cells stably expressing the indicated constructs were serum-starved for 6 h prior to drug treatment. Cells were treated as described in figure legends and then lysed in lysis buffer (50 mM Tris-HCl, pH 7.5, 300 mM NaCl, 1 mM EDTA, 1 mM Na_3VO_4, 1 mM NaF, 10% glycerol, phosphatase and protease inhibitors). For JNK and c-Jun experiments, buffer was supplemented with 1% Triton X-100. Lysates were sonicated and centrifuged (15,000 × *g*, 25 min, 4 °C), and the supernatant was stored at −20 °C. Total protein concentration was determined by BCA assay (Pierce) with BSA standards before loading 40 μg (JNK), 30 μg (c-Jun), 20 μg (ERK1/2), or 10 μg (arrestin) onto 10% Bis-Tris precast gels (Life Technologies) and running at 120 V for 1.5–2 h. Blots were transferred to nitrocellulose (Whatman) for 1.5 h at 30 V. Nitrocellulose was blocked with 5% BSA-TBST for 1 h at room temperature and stained overnight for c-Jun and phospho-c-Jun, JNK and phospho-JNK, ERK1/2 and phospho-ERK1/2, or arrestin 2 or 3 and actin. Blots were incubated in IRDye secondary antibody (LI-COR Biosciences, catalog number 926-68070, lot C50721-05 and catalog number 926-32211, lot C506602-05; 1:10,000) in 1:1 Odyssey buffer (LI-COR Biosciences) and 5% milk-TBST for 1 h at room temperature and then scanned on the Odyssey IR Imaging System (LI-COR Biosciences). Band intensity with background subtraction was measured using Odyssey software (Image Studio 3.1 and Image Studio Lite 4.0, LI-COR Biosciences). Phosphoprotein band intensity was normalized to total (ERK1/2 and c-Jun) or actin (JNK) band intensity. Data were normalized to

percentage of control sample (percent vehicle or percent basal) and plotted using GraphPad Prism 6.07 (GraphPad Software, Inc.). Statistical significance ($p < 0.05$) was determined by analysis of variance (ANOVA) followed by Holm–Šidák post hoc test.

Western antibody conditions

Phospho-JNK (Cell Signaling Technology, catalog number 9251, lot 26), phospho-ERK1/2 (Cell Signaling Technology, catalog number 9101, lot 28), phospho-c-Jun (Cell Signaling Technology, catalog number 9261, lot 14), c-Jun (Cell Signaling Technology, catalog number 2315, lot 3), and ERK2 (Santa Cruz Biotechnology, sc1647) antibodies were incubated at 1:1000 in 5% BSA-TBST overnight at 4 °C. Actin (Abcam AB8226, lot GR111289-6 or AB8227, lot GR168708-2) antibody was incubated at 1:5000 in 5% BSA-TBST. Arrestin 2 IR or arrestin 3 IR (antibody provided by Dr. Jeffrey Benovic, Thomas Jefferson University, Philadelphia, PA) (1:3000) was incubated in 5% BSA-TBST overnight at 4 °C.

Reactive oxygen species measured by CellROX Green fluorescence

Untransfected HEK293 cells or cells stably expressing mycKOR were grown on poly-D-lysine–treated coverslips the day prior to the experiment. For transient mycKOR and mycKOR(S369A) experiments, HEK293 cells were plated on coverslips 48 h prior to the experiment and transiently transfected with mycKOR or mycKOR(S369A) 24 h prior. Cells were serum-starved for 5 h and then treated as described. CellROX Green (10 μM; Molecular Probes) was added during the last 30 min of treatment. Cells were rinsed in PBS and fixed for 15 min with 4% paraformaldehyde. Cells were mounted on glass slides with VectaShield HardSet with DAPI (Vector Laboratories) and imaged within 12 h. Coverslips were imaged on a Nikon upright fluorescence microscope with Nikon Elements AR v3.1 software (Nikon Instruments). To prevent photoactivation, exposure to light during sample generation and imaging was minimized. Two representative fields from each coverslip were imaged for CellROX (488 nm) and DAPI. Exposure times were held constant for every fluorophore throughout the entire experiment. Image intensities for between 7 and 20 cells per image were quantified using ImageJ v 1.42q (National Institutes of Health), and these were averaged to give an average field intensity value. This was done for the two coverslip images and averaged to make one sample (*n*).

Reactive oxygen species measured by HyPerRed fluorescence

mycKOR-expressing or untransfected HEK293 cells grown on poly-D-lysine–coated coverslips were transiently transfected with HyPerRed using FuGENE HD. The following day, cells were serum-starved for 6 h and treated as described. Cells were blocked for 30 min with 1% BSA in PBS, 0.025% Triton X-100; incubated in rabbit anti-KOR antibody (70) at 1 μg/ml overnight at 4 °C; washed; and incubated with Alexa Fluor 488 anti-rabbit secondary (Life Technologies) for 1 h. Cells were washed, mounted on glass slides with VectaShield HardSet with DAPI, and stored at 4 °C until imaging. Coverslips were imaged on a Nikon upright fluorescence microscope at 10×. Repre-

sentative fields from each coverslip were imaged for KOR, HyPerRed (555 nm), and DAPI. Exposure times were held constant for every fluorophore throughout the experiment. Images were adjusted to a standard threshold value. Image intensities for between 20 and 40 cells per image were quantified using ImageJ v 1.42q (National Institutes of Health), and these were averaged to give an average field intensity value.

Live-cell imaging of HyPerRed fluorescence

HEK293 cells or cells stably expressing mycKOR were grown on chambered coverslips (Ibidi) 18 h prior to transient transfection with HyPerRed using FuGENE HD, and media were changed after 24 h. Cells were serum-starved for 6 h prior to the experiment, which took place 36–48 h after transfection. Cells were imaged on a Leica SP8X confocal microscope using LASX software at 20× with a 2× digital zoom, maintaining temperature in the imaged chambers at 34.9 °C (S.D., ±0.2 °C). Two treatment conditions were imaged in parallel for each experiment, tracking two fields per condition using the "hold focus" and "mark and track" functions, with scanning intervals of 60 s. Each replicate represents the average of the two positions in the well from each experiment. HyPerRed (excitation with WLL 577 laser at 10%, emission with HyD sensor at 584–692 with 0.3% gating and smart gain of 33.1%) and brightfield were imaged with 512×512 resolution, 600 speed with bidirectional scanning, and live averaging of 2. Ten frames were measured before the first drug treatment; cells were treated as described and treated with 200 μM H_2O_2 at the end of all experiments to confirm response with a positive control. MATLAB R2017a software was used for live-cell image processing. Fluorescence was quantified by averaging the pixel intensity across the whole frame. Background intensity was consistent with imaging noise and thus negligibly affected the average whole-frame intensity. A two-frame-window moving average was used to adjust for frame-to-frame fluorescence noise fluctuations in the time-course data.

Quantification and statistical analysis

GraphPad Prism 7.03 software was used for data analysis. Data are represented as mean ± S.E. When data are presented as percent baseline, percent vehicle, or -fold change, data were normalized to a within-replicate control set at 100%, which is represented by a dashed line. Statistical analyses are described in the corresponding figure legends.

References

1. Schwarzer, C. (2009) 30 years of dynorphins—new insights on their functions in neuropsychiatric diseases. *Pharmacol. Ther.* **123,** 353–370 CrossRef Medline

2. Bruchas, M. R., and Chavkin, C. (2010) Kinase cascades and ligand-directed signaling at the κ opioid receptor. *Psychopharmacology* **210,** 137–147 CrossRef Medline

3. Tejeda, H. A., Shippenberg, T. S., and Henriksson, R. (2012) The dynorphin/κ-opioid receptor system and its role in psychiatric disorders. *Cell. Mol. Life Sci.* **69,** 857–896 CrossRef Medline

4. Chavkin, C., and Koob, G. F. (2016) Dynorphin, dysphoria, and dependence: the stress of addiction. *Neuropsychopharmacology* **41,** 373–374 CrossRef Medline

5. Shippenberg, T. S., and Herz, A. (1986) Differential effects of μ and κ opioid systems on motivational processes. *NIDA Res. Monogr.* **75,** 563–566 Medline

6. Pfeiffer, A., Brantl, V., Herz, A., and Emrich, H. M. (1986) Psychotomimesis mediated by κ opiate receptors. *Science* **233,** 774–776 CrossRef Medline

7. Land, B. B., Bruchas, M. R., Lemos, J. C., Xu, M., Melief, E. J., and Chavkin, C. (2008) The dysphoric component of stress is encoded by activation of the dynorphin κ-opioid system. *J. Neurosci.* **28,** 407–414 CrossRef Medline

8. Ehrich, J. M., Messinger, D. I., Knakal, C. R., Kuhar, J. R., Schattauer, S. S., Bruchas, M. R., Zweifel, L. S., Kieffer, B. L., Phillips, P. E., and Chavkin, C. (2015) κ opioid receptor-induced aversion requires p38 MAPK activation in VTA dopamine neurons. *J. Neurosci.* **35,** 12917–12931 CrossRef Medline

9. Brust, T. F., Morgenweck, J., Kim, S. A., Rose, J. H., Locke, J. L., Schmid, C. L., Zhou, L., Stahl, E. L., Cameron, M. D., Scarry, S. M., Aubé, J., Jones, S. R., Martin, T. J., and Bohn, L. M. (2016) Biased agonists of the κ opioid receptor suppress pain and itch without causing sedation or dysphoria. *Sci. Signal.* **9,** ra117 CrossRef Medline

10. Schattauer, S. S., Kuhar, J. R., Song, A., and Chavkin, C. (2017) Nalfurafine is a G-protein biased agonist having significantly greater bias at the human than rodent form of the κ opioid receptor. *Cell. Signal.* **32,** 59–65 CrossRef Medline

11. Bals-Kubik, R., Ableitner, A., Herz, A., and Shippenberg, T. S. (1993) Neuroanatomical sites mediating the motivational effects of opioids as mapped by the conditioned place preference paradigm in rats. *J. Pharmacol. Exp. Ther.* **264,** 489–495 Medline

12. McLaughlin, J. P., Marton-Popovici, M., and Chavkin, C. (2003) κ opioid receptor antagonism and prodynorphin gene disruption block stress-induced behavioral responses. *J. Neurosci.* **23,** 5674–5683 CrossRef Medline

13. Mague, S. D., Pliakas, A. M., Todtenkopf, M. S., Tomasiewicz, H. C., Zhang, Y., Stevens, W. C., Jr., Jones, R. M., Portoghese, P. S., and Carlezon, W. A., Jr. (2003) Antidepressant-like effects of κ-opioid receptor antagonists in the forced swim test in rats. *J. Pharmacol. Exp. Ther.* **305,** 323–330 CrossRef Medline

14. McLaughlin, J. P., Li, S., Valdez, J., Chavkin, T. A., and Chavkin, C. (2006) Social defeat stress-induced behavioral responses are mediated by the endogenous κ opioid system. *Neuropsychopharmacology* **31,** 1241–1248 CrossRef Medline

15. Carlezon, W. A., Jr., Béguin, C., DiNieri, J. A., Baumann, M. H., Richards, M. R., Todtenkopf, M. S., Rothman, R. B., Ma, Z., Lee, D. Y., and Cohen, B. M. (2006) Depressive-like effects of the κ-opioid receptor agonist salvinorin A on behavior and neurochemistry in rats. *J. Pharmacol. Exp. Ther.* **316,** 440–447 CrossRef Medline

16. Knoll, A. T., and Carlezon, W. A., Jr. (2010) Dynorphin, stress, and depression. *Brain Res.* **1314,** 56–73 CrossRef Medline

17. Carroll, F. I., and Carlezon, W. A., Jr. (2013) Development of κ opioid receptor antagonists. *J. Med. Chem.* **56,** 2178–2195 CrossRef Medline

18. Chavkin, C., and Martinez, D. (2015) κ antagonist JDTic in phase 1 clinical trial. *Neuropsychopharmacology* **40,** 2057–2058 CrossRef Medline

19. McLaughlin, J. P., Myers, L. C., Zarek, P. E., Caron, M. G., Lefkowitz, R. J., Czyzyk, T. A., Pintar, J. E., and Chavkin, C. (2004) Prolonged κ opioid receptor phosphorylation mediated by G-protein receptor kinase underlies sustained analgesic tolerance. *J. Biol. Chem.* **279,** 1810–1818 CrossRef Medline

20. Xu, M., Petraschka, M., McLaughlin, J. P., Westenbroek, R. E., Caron, M. G., Lefkowitz, R. J., Czyzyk, T. A., Pintar, J. E., Terman, G. W., and Chavkin, C. (2004) Neuropathic pain activates the endogenous κ opioid system in mouse spinal cord and induces opioid receptor tolerance. *J. Neurosci.* **24,** 4576–4584 CrossRef Medline

21. McLennan, G. P., Kiss, A., Miyatake, M., Belcheva, M. M., Chambers, K. T., Pozek, J. J., Mohabbat, Y., Moyer, R. A., Bohn, L. M., and Coscia, C. J. (2008) κ opioids promote the proliferation of astrocytes via Gβγ and β-arrestin 2-dependent MAPK-mediated pathways. *J. Neurochem.* **107,** 1753–1765 CrossRef Medline

22. Schattauer, S. S., Miyatake, M., Shankar, H., Zietz, C., Levin, J. R., Liu-Chen, L. Y., Gurevich, V. V., Rieder, M. J., and Chavkin, C. (2012) Ligand directed signaling differences between rodent and human κ-opioid receptors. *J. Biol. Chem.* **287,** 41595–41607 CrossRef Medline

23. Bruchas, M. R., Macey, T. A., Lowe, J. D., and Chavkin, C. (2006) κ opioid receptor activation of p38 MAPK is GRK3- and arrestin-dependent in neurons and astrocytes. *J. Biol. Chem.* **281,** 18081–18089 CrossRef Medline

24. Bruchas, M. R., Schindler, A. G., Shankar, H., Messinger, D. I., Miyatake, M., Land, B. B., Lemos, J. C., Hagan, C. E., Neumaier, J. F., Quintana, A., Palmiter, R. D., and Chavkin, C. (2011) Selective p38α MAPK deletion in serotonergic neurons produces stress resilience in models of depression and addiction. *Neuron* **71,** 498–511 CrossRef Medline

25. Schindler, A. G., Messinger, D. I., Smith, J. S., Shankar, H., Gustin, R. M., Schattauer, S. S., Lemos, J. C., Chavkin, N. W., Hagan, C. E., Neumaier, J. F., and Chavkin, C. (2012) Stress produces aversion and potentiates cocaine reward by releasing endogenous dynorphins in the ventral striatum to locally stimulate serotonin reuptake. *J. Neurosci.* **32,** 17582–17596 CrossRef Medline

26. Abraham, A. D., Schattauer, S. S., Reichard, K. L., Cohen, J. H., Fontaine, H. M., Song, A. J., Johnson, S. D., Land, B. B., and Chavkin, C. (2018) Estrogen regulation of GRK2 inactivates κ opioid receptor signaling mediating analgesia, but not aversion. *J. Neurosci.* **38,** 8031–8043 CrossRef Medline

27. Bruchas, M. R., Yang, T., Schreiber, S., Defino, M., Kwan, S. C., Li, S., and Chavkin, C. (2007) Long-acting κ opioid antagonists disrupt receptor signaling and produce noncompetitive effects by activating c-Jun N-terminal kinase. *J. Biol. Chem.* **282,** 29803–29811 CrossRef Medline

28. Melief, E. J., Miyatake, M., Carroll, F. I., Béguin, C., Carlezon, W. A., Jr., Cohen, B. M., Grimwood, S., Mitch, C. H., Rorick-Kehn, L., and Chavkin, C. (2011) Duration of action of a broad range of selective κ-opioid receptor antagonists is positively correlated with c-Jun N-terminal kinase-1 activation. *Mol. Pharmacol.* **80,** 920–929 CrossRef Medline

29. Schattauer, S. S., Land, B. B., Reichard, K. L., Abraham, A. D., Burgeno, L. M., Kuhar, J. R., Phillips, P. E. M., Ong, S. E., and Chavkin, C. (2017) Peroxiredoxin 6 mediates Gαi protein-coupled receptor inactivation by cJun kinase. *Nat. Commun.* **8,** 743 CrossRef Medline

30. Melief, E. J., Miyatake, M., Bruchas, M. R., and Chavkin, C. (2010) Ligand-directed c-Jun N-terminal kinase activation disrupts opioid receptor signaling. *Proc. Natl. Acad. Sci. U.S.A.* **107,** 11608–11613 CrossRef Medline

31. Munro, T. A., Berry, L. M., Van't Veer, A., Béguin, C., Carroll, F. I., Zhao, Z., Carlezon, W. A., Jr., and Cohen, B. M. (2012) Long-acting κ opioid antagonists nor-BNI, GNTI and JDTic: pharmacokinetics in mice and lipophilicity. *BMC Pharmacol.* **12,** 5 CrossRef Medline

32. Kam, A. Y., Chan, A. S., and Wong, Y. H. (2004) Phosphatidylinositol-3 kinase is distinctively required for μ-, but not κ-opioid receptor-induced activation of c-Jun N-terminal kinase. *J. Neurochem.* **89,** 391–402 CrossRef Medline

33. Chavkin, C., James, I. F., and Goldstein, A. (1982) Dynorphin is a specific endogenous ligand of the κ opioid receptor. *Science* **215,** 413–415 CrossRef Medline

34. Suda, M., Nakao, K., Yoshimasa, T., Ikeda, Y., Sakamoto, M., Yanaihara, C., Yanaihara, N., Numa, S., and Imura, H. (1983) Comparison of the action of putative endogenous κ-agonists, leumorphin and rimorphin *in vitro*. *Life Sci.* **33,** Suppl. 1, 275–278 CrossRef Medline

35. Bian, J. S., Zhang, W. M., Pei, J. M., and Wong, T. M. (2000) The role of phosphodiesterase in mediating the effect of protein kinase C on cyclic AMP accumulation upon κ-opioid receptor stimulation in the rat heart. *J. Pharmacol. Exp. Ther.* **292,** 1065–1070 Medline

36. Zhou, J. J., Bian, J. S., Pei, J. M., Wu, S., Li, H. Y., and Wong, T. M. (2002) Role of protein kinase C-ε in the development of κ-opioid receptor tolerance to U50,488H in rat ventricular myocytes. *Br. J. Pharmacol.* **135,** 1675–1684 CrossRef Medline

37. Cao, C. M., Chen, M., and Wong, T. M. (2005) The K_{Ca} channel as a trigger for the cardioprotection induced by κ-opioid receptor stimulation—its relationship with protein kinase C. *Br. J. Pharmacol.* **145,** 984–991 CrossRef Medline

38. Bohn, L. M., Belcheva, M. M., and Coscia, C. J. (2000) Mitogenic signaling via endogenous κ-opioid receptors in C6 glioma cells: evidence for the involvement of protein kinase C and the mitogen-activated protein kinase signaling cascade. *J. Neurochem.* **74,** 564–573 CrossRef Medline

39. Munanairi, A., Liu, X. Y., Barry, D. M., Yang, Q., Yin, J. B., Jin, H., Li, H., Meng, Q. T., Peng, J. H., Wu, Z. Y., Yin, J., Zhou, X. Y., Wan, L., Mo, P., Kim, S., *et al.* (2018) Non-canonical opioid signaling inhibits itch transmission in the spinal cord of mice. *Cell Rep.* **23,** 866–877 CrossRef Medline

40. Kuhar, J. R., Bedini, A., Melief, E. J., Chiu, Y. C., Striegel, H. N., and Chavkin, C. (2015) μ opioid receptor stimulation activates c-Jun N-terminal kinase 2 by distinct arrestin-dependent and independent mechanisms. *Cell. Signal.* **27,** 1799–1806 CrossRef Medline

41. Jain, M. K., Tao, W. J., Rogers, J., Arenson, C., Eibl, H., and Yu, B. Z. (1991) Active-site-directed specific competitive inhibitors of phospholipase A2: novel transition-state analogues. *Biochemistry* **30,** 10256–10268 CrossRef Medline

42. Fisher, A. B., Dodia, C., Chander, A., and Jain, M. (1992) A competitive inhibitor of phospholipase A2 decreases surfactant phosphatidylcholine degradation by the rat lung. *Biochem. J.* **288,** 407–411 CrossRef Medline

43. Wang, R., Dodia, C. R., Jain, M. K., and Fisher, A. B. (1994) Purification and characterization of a calcium-independent acidic phospholipase A2 from rat lung. *Biochem. J.* **304,** 131–137 CrossRef Medline

44. Zhang, T., Inesta-Vaquera, F., Niepel, M., Zhang, J., Ficarro, S. B., Machleidt, T., Xie, T., Martin, J. A., Kim, N., Sim, T., Laughlin, J. D., Park, H., LoGrasso, P. V., Patricelli, M., Nomanbhoy, T. K., *et al.* (2012) Discovery of potent and selective covalent inhibitors of JNK. *Chem. Biol.* **19,** 140–154 CrossRef Medline

45. Ermakova, Y. G., Bilan, D. S., Matlashov, M. E., Mishina, N. M., Markvicheva, K. N., Subach, O. M., Subach, F. V., Bogeski, I., Hoth, M., Enikolopov, G., and Belousov, V. V. (2014) Red fluorescent genetically encoded indicator for intracellular hydrogen peroxide. *Nat. Commun.* **5,** 5222 CrossRef Medline

46. Appleyard, S. M., Celver, J., Pineda, V., Kovoor, A., Wayman, G. A., and Chavkin, C. (1999) Agonist-dependent desensitization of the κ opioid receptor by G protein receptor kinase and β-arrestin. *J. Biol. Chem.* **274,** 23802–23807 CrossRef Medline

47. McLaughlin, J. P., Xu, M., Mackie, K., and Chavkin, C. (2003) Phosphorylation of a carboxyl-terminal serine within the κ-opioid receptor produces desensitization and internalization. *J. Biol. Chem.* **278,** 34631–34640 CrossRef Medline

48. Land, B. B., Bruchas, M. R., Schattauer, S., Giardino, W. J., Aita, M., Messinger, D., Hnasko, T. S., Palmiter, R. D., and Chavkin, C. (2009) Activation of the κ opioid receptor in the dorsal raphe nucleus mediates the aversive effects of stress and reinstates drug seeking. *Proc. Natl. Acad. Sci. U.S.A.* **106,** 19168–19173 CrossRef Medline

49. Stefanoska, K., Bertz, J., Volkerling, A. M., van der Hoven, J., Ittner, L. M., and Ittner, A. (2018) Neuronal MAP kinase p38α inhibits c-Jun N-terminal kinase to modulate anxiety-related behaviour. *Sci. Rep.* **8,** 14296 CrossRef Medline

50. Costa-Neto, C. M., Parreiras-E-Silva, L. T., and Bouvier, M. (2016) A pluridimensional view of biased agonism. *Mol. Pharmacol.* **90,** 587–595 CrossRef Medline

51. Luttrell, L. M., Ferguson, S. S., Daaka, Y., Miller, W. E., Maudsley, S., Della Rocca, G. J., Lin, F., Kawakatsu, H., Owada, K., Luttrell, D. K., Caron, M. G., and Lefkowitz, R. J. (1999) β-Arrestin-dependent formation of β2 adrenergic receptor-Src protein kinase complexes. *Science* **283,** 655–661 CrossRef Medline

52. Luttrell, L. M., Wang, J., Plouffe, B., Smith, J. S., Yamani, L., Kaur, S., Jean-Charles, P. Y., Gauthier, C., Lee, M. H., Pani, B., Kim, J., Ahn, S., Rajagopal, S., Reiter, E., Bouvier, M., *et al.* (2018) Manifold roles of β-arrestins in GPCR signaling elucidated with siRNA and CRISPR/Cas9. *Sci. Signal.* **11,** eaat7650 CrossRef Medline

53. Halls, M. L., and Canals, M. (2018) Genetically encoded FRET biosensors to illuminate compartmentalised GPCR signalling. *Trends Pharmacol. Sci.* **39,** 148–157 CrossRef Medline

54. Eichel, K., and von Zastrow, M. (2018) Subcellular organization of GPCR signaling. *Trends Pharmacol. Sci.* **39,** 200–208 CrossRef Medline

55. Liu, J. J., Sharma, K., Zangrandi, L., Chen, C., Humphrey, S. J., Chiu, Y. T., Spetea, M., Liu-Chen, L. Y., Schwarzer, C., and Mann, M. (2018) *In vivo* brain GPCR signaling elucidated by phosphoproteomics. *Science* **360,** eaao4927 CrossRef Medline

56. Holmström, K. M., and Finkel, T. (2014) Cellular mechanisms and physiological consequences of redox-dependent signalling. *Nat. Rev. Mol. Cell Biol.* **15,** 411–421 CrossRef Medline

57. Dickinson, B. C., and Chang, C. J. (2011) Chemistry and biology of reactive oxygen species in signaling or stress responses. *Nat. Chem. Biol.* **7,** 504–511 CrossRef Medline

58. Hotamisligil, G. S., and Davis, R. J. (2016) Cell signaling and stress responses. *Cold Spring Harb. Perspect. Biol.* **8,** a006072 CrossRef Medline

59. Chen, K., Craige, S. E., and Keaney, J. F., Jr. (2009) Downstream targets and intracellular compartmentalization in Nox signaling. *Antioxid. Redox Signal.* **11,** 2467–2480 CrossRef Medline

60. Wilson, C., and González-Billault, C. (2015) Regulation of cytoskeletal dynamics by redox signaling and oxidative stress: implications for neuronal development and trafficking. *Front. Cell. Neurosci.* **9,** 381 CrossRef Medline

61. Doyle, T., Bryant, L., Muscoli, C., Cuzzocrea, S., Esposito, E., Chen, Z., and Salvemini, D. (2010) Spinal NADPH oxidase is a source of superoxide in the development of morphine-induced hyperalgesia and antinociceptive tolerance. *Neurosci. Lett.* **483,** 85–89 CrossRef Medline

62. Doyle, T., Esposito, E., Bryant, L., Cuzzocrea, S., and Salvemini, D. (2013) NADPH-oxidase 2 activation promotes opioid-induced antinociceptive tolerance in mice. *Neuroscience* **241,** 1–9 CrossRef Medline

63. Ibi, M., Matsuno, K., Matsumoto, M., Sasaki, M., Nakagawa, T., Katsuyama, M., Iwata, K., Zhang, J., Kaneko, S., and Yabe-Nishimura, C. (2011) Involvement of NOX1/NADPH oxidase in morphine-induced analgesia and tolerance. *J. Neurosci.* **31,** 18094–18103 CrossRef Medline

64. Volkow, N. D., and Li, T. K. (2004) Drug addiction: the neurobiology of behaviour gone awry. *Nat. Rev. Neurosci.* **5,** 963–970 CrossRef Medline

65. Pittenger, C., and Duman, R. S. (2008) Stress, depression, and neuroplasticity: a convergence of mechanisms. *Neuropsychopharmacology* **33,** 88–109 CrossRef Medline

66. Steptoe, A., and Kivimäki, M. (2012) Stress and cardiovascular disease. *Nat. Rev. Cardiol.* **9,** 360–370 CrossRef Medline

67. Schiavone, S., Jaquet, V., Trabace, L., and Krause, K. H. (2013) Severe life stress and oxidative stress in the brain: from animal models to human pathology. *Antioxid. Redox Signal.* **18,** 1475–1490 CrossRef Medline

68. Miller, M. W., and Sadeh, N. (2014) Traumatic stress, oxidative stress and post-traumatic stress disorder: neurodegeneration and the accelerated-aging hypothesis. *Mol. Psychiatry* **19,** 1156–1162 CrossRef Medline

69. Nayernia, Z., Jaquet, V., and Krause, K. H. (2014) New insights on NOX enzymes in the central nervous system. *Antioxid. Redox Signal.* **20,** 2815–2837 CrossRef Medline

70. Drake, C. T., Patterson, T. A., Simmons, M. L., Chavkin, C., and Milner, T. A. (1996) κ opioid receptor-like immunoreactivity in guinea pig brain: ultrastructural localization in presynaptic terminals in hippocampal formation. *J. Comp. Neurol.* **370,** 377–395 CrossRef Medline